

CHAPTER 3

Ferrofluid Lubrication of Slider Bearings with Variable Magnetic Field

CONTENTS

Symbols

- 3.1 Introduction
- 3.2 The Problem and its Mathematical Formulation
- 3.3 Solution
- 3.4 Numerical Results and Discussion
- 3.5 Conclusions

References

SYMBOLS

a	$\frac{h_2}{h_1}$
A	bearing length (m)
B	bearing breadth (m)
f	coefficient of friction
\bar{f}	dimensionless coefficient of friction defined in equation (3.29)
F	frictional force on the slider (N)
\bar{F}	dimensionless frictional force defined in equation (3.28)
h	film thickness (m)
\bar{h}	dimensionless quantity defined in equation (3.21)
h_1, h_2	minimum and maximum values of h (m)
\dot{h}_1	squeeze velocity, $\frac{dh_1}{dt}$ (m s ⁻¹)
H	magnetic field strength (A m ⁻¹)
\mathbf{H}	magnetic field vector
I	sum of moments of inertia of the particles per unit volume (Ns ² m ⁻²)
I^*, I^{**}	integrals defined in equations (3.31), (3.32)
K	quantity defined in equation (3.12) (A m ⁻³)
k_B	Boltzmann constant (J (°K) ⁻¹)
m	magnetic moment of a particle (A m ²)
\mathbf{M}	magnetization vector

M_0	saturation magnetization ($A\ m^{-1}$)
n	number of particles per unit volume (m^{-3})
p	film pressure ($N\ m^{-2}$)
\bar{p}	dimensionless film pressure defined in equation (3.21)
$\mathbf{q} = (u, 0, w)$	fluid velocity vector
t	time (s)
T	temperature ($^{\circ}K$)
U	slider velocity ($m\ s^{-1}$)
W	load-carrying capacity (N)
\bar{W}	dimensionless load-carrying capacity defined equation (3.27)
x, y, z	coordinates
\bar{x}	x -coordinates of the center of pressure (m)
$\bar{\bar{x}}$	dimensionless center of pressure defined in equation (3.30)
X	$\frac{x}{A}$

Greek symbols

α	inclination of the magnetic field with the x -axis
β	squeeze velocity parameter defined in equation (3.21)
δ	central thickness of the convex pad (m)
$\bar{\delta}$	$\frac{\delta}{h_1}$

η	viscosity of the suspension (N s m^{-2})
η_0	viscosity of the liquid carrier (N s m^{-2})
λ	magnetic field strength parameter defined in equation (3.23)
μ_0	permeability of free space
ξ	dimensionless field strength (Langevin's parameter)
τ	rotational viscosity parameter
$\bar{\tau}$	defined in equation (3.10) (s)
τ_B	Brownian relaxation time (s)
τ_s	magnetic moment relaxation time (s)
$\mathbf{\Omega}$	$\frac{1}{2} \nabla \times \mathbf{q}$
φ	volume concentration of the particles

3.1 INTRODUCTION

Slider bearings, in general, are the oldest and simplest bearing technology with wide range of applications. It is generally used as a part in the composite system of machine used in many applications, for example – construction machinery, machines with atomic resolution, propeller, pumps, engines and automobile industries, etc. It has good resistance to wear, fatigue and corrosion with sufficient strength to support the load. The simplest hydrodynamic system is the plane slider used in the thrust bearings, journal bearing, etc. However, slider bearings have disadvantage of higher lubricant requirement due to large contact area. But with the use of ferrofluid (FF) lubricant this disadvantage can be discarded because of tendency of FF to retain at the required active contact zone under the influence of magnetic field effect. A FF or magnetic fluid (MF) is a colloidal dispersion of nano magnetic particles in a non-conducting carrier liquid. The important property of FF is that, under the influence of applied magnetic field, it can be made to adhere to any desired location on the surface, and due to this reason FF gained widespread popularity among the researchers working on lubrication theory of bearings. Thus, the use of FF lubrication also adds an additional importance from nano science point of view. Moreover, when the angular velocities of rotations of the carrier liquid as well as magnetic particles are different, frictional forces arise. These forces cause an increase in the effective viscosity of the FF, and it has major impact on the increase of pressure when FF is used as lubricant. Shliomis [1] studied the above effects of rotations of the carrier liquid as well as magnetic particles in the FF flow description in addition to magnetic body force. Jenkins [2-4] presented isothermal static equilibrium theory for FFs. Here, the spin component, which is parallel to the magnetization, is ignored. In comparison with Neuringer-Rosensweig (NR) FF flow model [5], Jenkins model distinguishes the volume force density (due to the self-field) from the external body force. NR model considers only magnetic body force and did not consider any

rotation effect. Huge amount of work on NR as well as Jenkins models have been carried out on lubrication theory as compared to Shliomis model. For recent updates on FF lubrication, the following are some references related to above three models.

The NR model is depended on the assumption that the magnetization vector is parallel to the magnetic field vector. It is used by many authors [6-14] from different viewpoints to study lubrication of different bearings. All have shown that the better performances of the bearing characteristics are obtained owing to use of FF as lubricant. Tipei [6] analyzed general momentum equations under the assumption of FFs as Newtonian fluids. The short bearing case is studied. It is shown that the load-carrying capacity increases because of the effect of magnetic particles. The bearing stability and stiffness are also shown to be improved. Agrawal [7] studied the effects of MF on a porous inclined slider bearing. It is shown that the load-carrying capacity increases without affecting the friction on the moving slider due to the effect of magnetization of the magnetic particles in the lubricant. Chi *et. al.* [8] studied new type of FF lubricated journal bearing consists of three pads (one of them is a deformable elastic pad). The theoretical analysis and experimental investigation shows the better performance of the bearing as compared to ordinary bearings (which uses conventional lubricant). Moreover, the bearing is operated without leakage and any feed system. Prajapati [9] analyzed effect of MF on different shapes of squeeze film bearing designs like circular, annular, elliptic, conical, etc. It is shown that the load-carrying capacity increases with the increase of magnetization parameter. It is also shown that the bearing with MF can support a load even when there is no flow. Shah and Bhat [10] analyzed FF lubricated squeeze film in a long journal bearing and concluded that as compared to Jenkins model, load-carrying capacity and response time are more in NR model. Also, it is shown that when magnetic field is uniform, the rotational viscosity parameter of Shliomis model causes increase in the load-carrying capacity and response time. Moreover, the non-uniform case of magnetic field is

also studied. Ahmad and Singh [11] discussed MF based porous pivoted slider bearings with the effect of slip velocity. The bearing characteristics like load-carrying capacity and center of pressure are studied. It is shown that load-carrying capacity increases with the increase of magnetic parameter, whereas it decreases with the increase of slip parameter and permeability parameter. Shah and Patel [12] discussed effects of various and arbitrary porous structures in the study of squeeze step bearing lubricated with MF using variable magnetic field. It is concluded that the load-carrying capacity increases with the increase of length of the first step as well as with the increase of magnetic field strength. Recently, Shah and Kataria [13] theoretically discussed FF based squeeze film between a sphere and a flat plate. It is concluded that loss in the dimensionless load-carrying capacity due to the effect of porosity is almost zero because of using FF as lubricant for smaller values of thickness parameter of the porous layer and radial permeability parameter. Shah and Patel [14] studied squeeze film characteristics between a rotating sphere and a radially rough plate using FF lubricant. It is shown that better performance of the dimensionless load-carrying capacity is obtained with respect to various parameters.

The Jenkins model is used by Ram and Verma [15] using simplification suggested by Maugin [16] to study FF lubrication of a porous inclined slider bearing. They found that due to the effects of FF and material parameter, the pressure and load-carrying capacity increases. The assumption of magnetization vector parallel to the magnetic field vector was made in the study. But studies of Shah and Bhat [17,18] shown that increase in the material parameter caused decrease in the load-carrying capacity and increase in the frictional force as well as the coefficient of friction. More recently, Shah and Patel [19] studied MF lubrication of a porous pivoted slider bearing with the effects of slip and squeeze velocity. It is concluded that load-carrying capacity can be improved substantially in the presence of squeeze velocity for smaller values of permeability parameter and increasing values of magnetic field strength.

Shukla and Kumar [20] used Shliomis model to study the slider and squeeze film bearings with uniform transverse magnetic field by neglecting relaxation time of particle rotation. They derived the pressure equation under the assumptions that the FF is saturated so that the saturation magnetization is independent of the applied magnetic field, and the magnetic moment relaxation time is negligible. However, Shah and Bhat [21] derived the pressure equation without above assumptions. The case of squeeze film between curved annular plates bearing is studied. It is concluded that the load-carrying capacity and approaching time of squeeze film can be enhanced by increasing the volume concentration of the solid phase in FF and the intensity of external magnetic field. Shah and Parikh [22] discussed different shapes of slider bearings. The dimensionless load-carrying capacity with and without using the effect of squeeze velocity are compared. It is concluded that the load capacity of all bearings remains constant with the increase of Langevin's parameter, whereas it has an increasing tendency with the increase of volume concentration of the particles. Singh and Gupta [23] studied FF based curved slider bearing with the effect of transverse magnetic field. It is shown that the effects of rotation and volume concentration of the magnetic particles improve the stiffness and damping capacities of the bearing. Recently, Lin [24] derived Reynolds equation for MF lubricated slider bearings using transverse magnetic field. It is shown that load-carrying capacity, dynamic stiffness and damping characteristics are improved.

All above studies based on Shliomis FF flow model are with transverse magnetic field. However, the study of slider bearings with oblique radially variable magnetic field with squeeze velocity is ignored. The variable magnetic field is important because of its advantage of generating maximum field at the required active contact zone in the bearing design system. The squeeze effect is included because it generates an additional pressure. The Shliomis model is considered because it behaves differently in the case of variable magnetic field.

Hence, there is a need of the present study. Thus, the present study considers Shliomis model with the effects of oblique radially variable magnetic field and squeeze velocity to derive modified Reynolds equation for the study of lubrication of different slider bearings. Different slider bearing designs are made up of various stators shapes (inclined, exponential, secant, convex and parallel) and flat parallel sliders. While deriving Reynolds equation, continuity equation is used for the film region. Using Reynolds equation, general form of pressure equation is derived and expressions for dimensionless load-carrying capacity, frictional force, coefficient of friction and center of pressure are obtained. Using these expressions, results for different slider bearings are computed for different parameters and compared. The pressure equation derived in the present case is of more general nature and different than all previous studies [20-24]. The case of sample magnetic field is considered in the present analysis. However, the study with other forms of magnetic field can be discussed similarly.

3.2 THE PROBLEM AND ITS MATHEMATICAL FORMULATION

Figures 3.1-3.5 shows physical configuration of the different slider bearing designs under consideration, which are infinite in y -direction. The lower surface is a slider of length A along the x -axis and moving with uniform velocity U in x -direction. The upper surface is a stator of various shapes (inclined pad, exponential pad, secant pad, convex pad and parallel pad) and having a normal velocity (known as squeeze velocity) \dot{h}_1 , where h_1 being the minimum value of the film thickness h . The maximum value of h is h_2 and B is the bearing breadth with $A \ll B$. As shown in figures the gap between slider and stator is known as film region and is filled with FF lubricant.

With usual assumptions of lubrication, steady flow, neglecting inertia terms and the second derivative of the internal angular momentum \bar{S} , the equations governing the FF flow by Shliomis model [1,21] are as follows.

Equation of Motion

$$-\nabla p + \eta \nabla^2 \mathbf{q} + \mu_0 (\mathbf{M} \cdot \nabla) \mathbf{H} + \frac{1}{2\tau_s} \nabla \times (\bar{\mathbf{S}} - I\boldsymbol{\Omega}) = 0, \quad (3.1)$$

Equation of Internal Angular Momentum

$$\bar{\mathbf{S}} = I\boldsymbol{\Omega} + \mu_0 \tau_s (\mathbf{M} \times \mathbf{H}), \quad (3.2)$$

Equation of Magnetization

$$\mathbf{M} = M_0 \frac{\mathbf{H}}{H} + \frac{\tau_B}{I} (\bar{\mathbf{S}} \times \mathbf{M}), \quad (3.3)$$

Equation of Continuity

$$\nabla \cdot \mathbf{q} = 0, \quad (3.4)$$

Maxwell's equations

$$\nabla \times \mathbf{H} = 0, \quad (3.5)$$

$$\nabla \cdot (\mathbf{M} + \mathbf{H}) = 0, \quad (3.6)$$

where p is the pressure, η is the viscosity of the suspension, μ_0 is the permeability of free space, \mathbf{H} is the applied magnetic field vector, H is magnetic field strength, \mathbf{M} is the magnetization vector, $\mathbf{q} = (u, 0, w)$ is the fluid velocity, I is the sum of moments of inertia of the particles per unit volume, $\boldsymbol{\Omega} = \frac{1}{2} \nabla \times \mathbf{q}$, τ_B is the Brownian relaxation time, τ_s is the magnetic moment relaxation time and M_0 is the equilibrium magnetization.

Using equation (3.2), equations (3.1) and (3.3) becomes

$$-\nabla p + \eta \nabla^2 \mathbf{q} + \mu_0 (\mathbf{M} \cdot \nabla) \mathbf{H} + \frac{\mu_0}{2} \nabla \times (\mathbf{M} \times \mathbf{H}) = 0 \quad (3.7)$$

and

$$\mathbf{M} = M_0 \frac{\mathbf{H}}{H} + \tau_B \boldsymbol{\Omega} \times \mathbf{M} - \frac{\mu_0 \tau_B \tau_s}{I} \mathbf{M} \times (\mathbf{M} \times \mathbf{H}). \quad (3.8)$$

For a strong magnetic field τ_s cannot be neglected (however, Shukla and Kumar [20] neglected τ_s in their analysis). Then equation (3.8) can be approximated as (refer [1,21])

$$\mathbf{M} = \frac{M_0}{H} (\mathbf{H} + \bar{\tau} \boldsymbol{\Omega} \times \mathbf{H}), \quad (3.9)$$

where

$$\bar{\tau} = \frac{\tau_B}{1 + (\mu_0 M_0 H \tau_B \tau_s / I)}. \quad (3.10)$$

Choose an external oblique radially variable magnetic field similar to [12]

$$\mathbf{H} = H(x)(\cos \alpha, 0, \sin \alpha) \quad (3.11)$$

with magnetic field strength

$$H(x) = K x (A - x) \quad (3.12)$$

as shown in figures 3.1-3.5 for considering active contact zone in the neighbourhood of $x = A/2$, where K being a quantity chosen to suit the dimensions of both sides of equation (3.12). Such a field attains maximum at $x = A/2$ and vanishes at $x = 0$ and $x = A$. Also, α being inclination of the magnetic field with the x -axis. This is the case of one sample magnetic field. For other active contact zones, suitable form of magnetic field strength can be chosen.

By assuming that the velocity gradient across the film predominate, equation (3.9) for small α and $\boldsymbol{\Omega} = \frac{1}{2} \nabla \times \mathbf{q}$ implies

$$\mathbf{M} \times \mathbf{H} = -M_0 H \bar{\tau} \mathbf{\Omega}. \quad (3.13)$$

The x -component of the equation (3.7), using equation (3.9) and (3.13), implies

$$-\frac{\partial p}{\partial x} + \eta \frac{\partial^2 u}{\partial z^2} + \mu_0 M_0 \frac{dH}{dx} + \frac{\mu_0 M_0 H \bar{\tau}}{4} \frac{\partial^2 u}{\partial z^2} = 0, \quad (3.14)$$

which on simplification yields

$$\frac{\partial^2 u}{\partial z^2} = \frac{1}{\eta \left(1 + \frac{\mu_0 M_0 H \bar{\tau}}{4\eta} \right)} \left(\frac{dp}{dx} - \mu_0 M_0 \frac{dH}{dx} \right). \quad (3.15)$$

Defining the following quantities for a suspension of spherical particles [1,21]

$$M_0 = nm(\coth \zeta - \frac{1}{\zeta}), \quad \zeta = \frac{\mu_0 m H}{k_B T}, \quad \tau_B = \frac{3\eta V}{k_B T}, \quad V = \frac{\varphi}{n}, \quad \tau_s = \frac{I}{6\eta\varphi}, \quad \tau = \frac{3}{2} \varphi \frac{\zeta - \tanh \zeta}{\zeta + \tanh \zeta}, \quad (3.16)$$

equation (3.15) takes the form

$$\frac{\partial^2 u}{\partial z^2} = \frac{1}{\eta(1+\tau)} \frac{d}{dx} \left(p - nk_B T \ln \frac{\sinh \zeta}{\zeta} \right), \quad (3.17)$$

where n, m, k_B, T, φ and τ are respectively the number of particles per unit volume, magnetic moment of a particle, Boltzmann constant, temperature, volume concentration of the particles and the rotational viscosity parameter.

Solving equation (3.17) under the no-slip boundary conditions [25,26]

$$u = U \quad \text{when } z = 0, \quad u = 0 \quad \text{when } z = h, \quad (3.18)$$

yields

$$u = U \left(1 - \frac{z}{h} \right) + \frac{z(z-h)}{2\eta(1+\tau)} \frac{d}{dx} \left(p - nk_B T \ln \frac{\sinh \xi}{\xi} \right). \quad (3.19)$$

Substituting equation (3.19) into the integral form of continuity equation (3.4) for the film region

$$\frac{\partial}{\partial x} \int_0^h u \, dz + w_h - w_0 = 0,$$

the modified Reynolds equation obtained for the present study as

$$\frac{d}{dx} \left[\frac{h^3}{(1+\tau)(1+\frac{5}{2}\varphi)} \frac{d}{dx} \left(p - nk_B T \ln \frac{\sinh \xi}{\xi} \right) \right] = 6\eta_0 U \frac{dh}{dx} + 12\eta_0 \dot{h}_1, \quad (3.20)$$

where $w_h = \dot{h}_1$ (squeeze velocity), $w_0=0$ (as the lower plate is impermeable) and

$$\eta = \eta_0 \left(1 + \frac{5}{2} \varphi \right),$$

which is the viscosity of the suspension in which η_0 is the viscosity of the carrier liquid.

3.3 SOLUTION

Introducing the dimensionless quantities

$$X = \frac{x}{A}, \quad \bar{h} = \frac{h}{h_1}, \quad \bar{p} = \frac{h_1^2 p}{\eta_0 U A}, \quad \beta = -\frac{2A\dot{h}_1}{Uh_1}, \quad \mu^* = \frac{nk_B T h_1^2}{\eta_0 U A} \quad (3.21)$$

and using equation (3.12), equation (3.20) becomes

$$\frac{d}{dX} \left[G \frac{d}{dX} \left\{ \bar{p} - \mu^* \ln \left(\frac{\sinh \xi}{\xi} \right) \right\} \right] = 6 \frac{d}{dX} (\bar{h} - \beta X), \quad (3.22)$$

where

$$G = \frac{\bar{h}^3}{(1+\tau)(1+\frac{5}{2}\varphi)}, \quad \xi = \lambda X(1-X), \quad \lambda = \frac{\mu_0 m K A^2}{k_B T}. \quad (3.23)$$

Solving equation (3.22) under the boundary conditions [25,26]

$$\bar{p} = 0 \quad \text{when} \quad X = 0, 1, \quad (3.24)$$

yields

$$\bar{p} = \mu^* \ln\left(\frac{\sinh \xi}{\xi}\right) + 6 \int_0^X \frac{\bar{h} - \beta X + Q}{G} dX, \quad (3.25)$$

where

$$Q = \frac{\int_0^1 \frac{\beta X - \bar{h}}{G} dX}{\int_0^1 \frac{dX}{G}}. \quad (3.26)$$

The load-carrying capacity W of the bearing, frictional force F on the slider, the coefficient of the friction f and the position \bar{x} of the center of pressure are defined, respectively as

$$W = \int_0^B \int_0^A p dx dy, \quad F = \eta \int_0^B \int_0^A \left. \frac{\partial u}{\partial z} \right|_{z=h} dx dy, \quad f = \frac{F}{W}, \quad \bar{x} = \frac{\int_0^B \int_0^A x p dx dy}{\int_0^B \int_0^A p dx dy}$$

and can be expressed in dimensionless forms as

$$\bar{W} = \frac{h_1^2 W}{\eta_0 U A^2 B} = \mu^* I^* - 6 \int_0^1 \frac{X}{G} (\bar{h} - \beta X + Q) dX, \quad (3.27)$$

$$\bar{F} = \frac{h_1 F}{\eta_0 UAB} = \left(1 + \frac{5}{2} \varphi\right) \int_0^1 \left[\frac{1}{h} + \frac{3}{h^2} (\bar{h} - \beta X + Q) \right] dX, \quad (3.28)$$

$$\bar{f} = \frac{Af}{h_1} = \frac{\bar{F}}{\bar{W}}, \quad (3.29)$$

$$\bar{\bar{x}} = \frac{\bar{x}}{A} = \frac{1}{2\bar{W}} \left[\mu^* I^{**} - 6 \int_0^1 \frac{X^2}{G} (\bar{h} - \beta X + Q) dX \right], \quad (3.30)$$

where

$$I^* = \lambda \int_0^1 X(1-2X) \left(\frac{1}{\zeta} - \coth \zeta \right) dX, \quad (3.31)$$

$$I^{**} = \lambda \int_0^1 X^2(1-2X) \left(\frac{1}{\zeta} - \coth \zeta \right) dX. \quad (3.32)$$

3.4 NUMERICAL RESULTS AND DISCUSSION

The values of the bearing characteristics \bar{W} , \bar{F} , \bar{f} and $\bar{\bar{x}}$ given by equations (3.27)-(3.30), respectively are computed using Simpson's one-third rule with step size 0.1 for different values of the magnetic field strength parameter λ and squeeze velocity parameter β for various stators shapes (inclined pad, exponential pad, secant pad, convex pad and parallel pad).

The representative values of the parameters taken in computation are [21,25]

$$a = 2, \quad A = 0.02 \text{ m}, \quad h_1 = 0.000025 \text{ m}, \quad k_B = 1.38 \times 10^{-23} \text{ J}(\text{K})^{-1},$$

$$T = 297 \text{ } ^\circ\text{K}, \quad \mu_0 m = 1.75 \times 10^{-25} \text{ JA}^{-1}\text{m}, \quad U = 6.28 \text{ ms}^{-1},$$

$$\varphi = 0.0075, \quad V = 1.02 \times 10^{-25} \text{ m}^3, \quad \eta_0 = 1.2 \times 10^{-2} \text{ Ns m}^{-1}, \quad \bar{\delta} = 0.06$$

$$\dot{h}_1 = -0.02 \text{ (ms}^{-1}\text{) (whenever fixed) } H \approx O(10^3) \text{ (whenever fixed)}$$

with the relations

$$\lambda = 4 \max \xi, \quad K = 2.3429 \times 10^8 \max \xi \text{ (A m}^{-3}\text{)}.$$

Also, for smaller values of ξ ,

$$\coth \xi - \frac{1}{\xi} \rightarrow 0, \quad \frac{\xi - \tanh \xi}{\xi + \tanh \xi} \rightarrow 0.$$

The calculation of magnetic field strength is shown below:

From equation (3.12),

$$H = K x (A - x)$$

$$\text{Max } H = 10^{-4} K$$

$$\text{For } H = O(10^4), \quad K = O(10^8)$$

With reference to the various stators shapes (inclined pad, exponential pad, secant pad, convex pad and parallel pad), the slider bearing designs referred here as inclined slider bearing, exponential slider bearing, secant slider bearing, convex slider bearing and parallel slider bearing, respectively. Accordingly using subscripts i, e, s, c, p , the following shapes are taken in computation.

$$\bar{h} = \bar{h}_i = a - (a-1)X; \quad 0 \leq X \leq 1$$

$$\bar{h} = \bar{h}_e = a \exp(-X \ln a); \quad 0 \leq X \leq 1$$

$$\bar{h} = \bar{h}_s = \sec\left\{\frac{\pi}{2}(1-X)\right\}; \quad 0 < X \leq 1$$

$$\bar{h} = \bar{h}_c = 4\bar{\delta}X^2 - (a-1+4\bar{\delta})X + a; \quad 0 \leq X \leq 1$$

$$\bar{h} = \bar{h}_p = 1; \quad 0 \leq X \leq 1$$

where

$$a = \frac{h_2}{h_1}, \quad \bar{\delta} = \frac{\delta}{h_1}$$

and δ is the central thickness of the convex pad.

The computed results for different bearing characteristics are displayed graphically in figures 3.6-3.13.

Figures 3.6 and 3.7 show the variations in dimensionless center of pressure \bar{x} as a function of magnetic field strength parameter λ and squeeze velocity parameter β , respectively for different slider bearing designs. The position of \bar{x} shift towards the outlet for all bearing designs except parallel. The shifting is maximum in the case of secant slider bearing. For parallel slider bearing, \bar{x} is in the middle of the bearing. It should be noted here that for inclined, exponential and convex slider bearings, the position of \bar{x} remains almost same, and it is inbetween secant and parallel slider bearings. It is also observed from the figures that the behaviour of \bar{x} remains constant with the increasing values of λ as well as β for all bearing designs. The overall behaviour of \bar{x} is obtained with respect to the corresponding behaviour of dimensionless load-carrying capacity \bar{W} as shown in figures 3.8 and 3.9 under similar conditions. Table 3.1 shows the exact shifting of \bar{x} for different bearing designs with the corresponding values of \bar{W} . The position of \bar{x} has significant impact on dimensionless load-carrying capacity \bar{W} , and hence on the dimensionless coefficient of friction \bar{f} .

Figures 3.8 and 3.9 show the variations in dimensionless load-carrying capacity \bar{W} as a function of λ and β , respectively for different slider bearing designs. It is observed that \bar{W} is maximum for parallel slider bearing, whereas it is least for secant slider bearing (refer Table 3.1 also). For all other bearings, \bar{W} almost remains the same. This behaviour of \bar{W} agrees with the results of [22] when uniform transverse magnetic field is used, but the present analysis is having advantage of possibility of generating maximum magnetic field at the required active contact zone of the bearing design system. It can be seen from Table 3.2 that the percentage increase in \bar{W} for parallel slider bearing as compared to secant slider bearing is 363.93%, which is maximum among all the considered slider bearings. For all other bearings the percentage increase rate varies from 76.43-88.93%. Moreover, it is further observed that the behaviour of \bar{W} remains constant with the increasing values of λ , whereas it is increasing with the increasing values of β ; that is, \bar{W} increases with the increase of squeeze velocity.

Referring to [22], parallel slider bearing cannot support a load when FF is used as lubricant using uniform transverse magnetic field and no squeeze velocity. But with the effect of squeeze velocity it supports a load. In the present analysis parallel slider bearing supports a load even if there is no squeeze velocity (refer Table 3.3). Moreover, it increases with the increase of λ ; that is, with the increase of magnetic field strength. Thus, additional advantage is obtained in the present study.

It should be noted from figures 3.6 - 3.9 that only for parallel slider bearing the center of pressure is at the middle; that is, at $x = A/2$. Also, the magnetic field considered in our study attains maximum at $x = A/2$. Thus, center of pressure and maximum magnetic field coincide at $x = A/2$, which results into the maximum load-carrying capacity of parallel slider bearing. For all other bearings the center of pressure shifts towards the outlet and so load-carrying capacity is reduced as compared to parallel slider bearing. The load-carrying

capacity is least in the case of secant slider bearing because the shifting of center of pressure is maximum towards the outlet as compared to other bearing designs.

Figures 3.10 and 3.11 show the variations in dimensionless frictional force \bar{F} as a function of λ and β , respectively for different slider bearing designs. It is observed that \bar{F} is least for parallel slider bearing, whereas it is maximum for inclined, exponential and convex slider bearings when $\beta > 2.55$. Moreover, \bar{F} almost remains the same in all these three cases. The behaviour of \bar{F} remains constant with the increasing values of λ for all bearing designs, whereas it is increasing with the increasing values of β except for parallel slider bearing. For parallel slider bearing the behaviour of \bar{F} remains constant. Table 3.4 shows that the percentage increase rate in \bar{F} varies from 8.50-11.66% for inclined, convex and exponential slider bearings as compared to secant slider bearing. Moreover, it is maximum 11.66% for exponential slider bearing. For parallel slider bearing reverse trend is obtained and \bar{F} decreased by 7.87% as compared to secant slider bearing.

Figures 3.12 and 3.13 show the variations in dimensionless coefficient of friction \bar{f} as a function of λ and β , respectively for different slider bearing designs. It is observed that \bar{f} is least in the case of parallel slider bearing, whereas it is maximum for secant slider bearing. For all other bearings, \bar{f} is almost remains the same. Moreover, for all bearing designs the behaviour of \bar{f} remains constant with the increasing values of λ , whereas it is decreasing with the increasing values of β . This behaviour of \bar{f} is obtained with respect to the corresponding behaviour of \bar{F} in figures 3.10 and 3.11, and \bar{W} in figures 3.8 and 3.9 under similar conditions. Table 3.5 shows that as compared to secant slider bearing, for all other bearings \bar{f} decreases from 38.47-80.13%. For parallel slider bearing, the percentage decrease rate of \bar{f} is maximum of 80.13%.

It can also be observed from the above discussion that parallel and secant slider bearings have opposite behaviour for all bearing characteristics except frictional force. Inclined, exponential and convex slider bearings have almost same behaviour for all bearing characteristics.

3.5 CONCLUSIONS

Based on the Shliomis model for FF flow and continuity equation, modified Reynolds equation for the study of lubrication of different slider bearings, is derived for the general shape $h = h(x, t)$ by considering the effects of oblique radially variable magnetic field and squeeze velocity. Different slider bearing designs are made up of various stators shapes (inclined, exponential, secant, convex and parallel) and flat parallel sliders. The Shliomis model is important because it includes the effects of rotations of the carrier liquid as well as magnetic particles. Moreover, Shliomis model behaves differently in the case of variable magnetic field in the sense that the pressure equation derived in the present study is of more general nature and different than all previous studies. The variable magnetic field is important because of its advantage of generating maximum field at the required active contact zone. The squeeze effect is included because it generates an additional pressure. Using Reynolds equation, general form of pressure equation is derived and expressions for dimensionless load-carrying capacity (\bar{W}), frictional force (\bar{F}), coefficient of friction (\bar{f}) and center of pressure (\bar{x}) are obtained. Using these expressions, results for different slider bearings are computed for different parameters and compared. In the present analysis, the case of sample magnetic field is considered in such a way that it is maximum at the middle of the bearing. However, the study with other forms of magnetic field because of different requirements can be discussed similarly. From the results and discussion, following conclusions can be made.

(1) \bar{W} is maximum for parallel slider bearing, whereas it is least for secant slider bearing.

For all other bearings, \bar{W} almost remains the same. Thus,

$$\bar{W}_p > \bar{W}_i \approx \bar{W}_e \approx \bar{W}_c > \bar{W}_s .$$

The behaviour of \bar{W} increases with the increasing values of squeeze velocity parameter β for all bearing designs.

(2) \bar{F} is maximum for inclined, exponential and convex slider bearings, whereas it is least for parallel slider bearing. Thus,

$$\bar{F}_p < \bar{F}_s < \bar{F}_i \approx \bar{F}_e \approx \bar{F}_c .$$

The behaviour of \bar{F} remains constant for parallel slider bearing, whereas it increases for all other bearings with the increasing values of β .

(3) \bar{f} is maximum for secant slider bearing, whereas it is least for parallel slider bearing. For all other bearings, \bar{f} almost remains the same. Thus,

$$\bar{f}_p < \bar{f}_i \approx \bar{f}_e \approx \bar{f}_c < \bar{f}_s .$$

The behaviour of \bar{f} decreases with the increasing values of β for all bearing designs.

(4) The position of \bar{x} shift towards the outlet for all bearing designs except parallel. The shifting is maximum in the case of secant slider bearing. For parallel slider bearing, \bar{x} is in the middle of the bearing. For inclined, exponential and convex slider bearings, the position of \bar{x} remains the same, and it is inbetween secant and parallel slider bearings. The behaviour of \bar{x} remains constant with the increasing values of β for all bearing designs.

- (5) The behaviour of \bar{W} , \bar{F} , \bar{f} and \bar{x} remains constant with the increasing values of λ for all bearing designs.
- (6) Maximum load-carrying capacity can be obtained when maximum magnetic field and center of pressure coincide.
- (7) The present model with oblique radially variable magnetic field supports load for parallel slider bearing even if there is no squeeze velocity, whereas in the case of uniform transverse magnetic field it does not support a load [22].
- (8) Present analysis is having advantage of possibility of generating maximum magnetic field at the required active contact zone of the bearing design system.

The FF based bearings are important mainly because of their high speed, less noise and auto sealing properties. In particular, the study of FF lubricated slider bearings are important because they are multipurpose bearings used as a part of many composite system. This study is necessary because under the influence of variable magnetic field, FFs can be forced to retain at the desired location. This location may be of different nature depends on application and in that case variable magnetic field is necessary for strengthening the FF spikes in particular direction. Thus, the present chapter serves direction for more general study and adds an important concept to lubrication theory from nano science point of view as it introduces Shliomis based FF flow model controlled by variable magnetic field. The results obtained indicates that while designing slider bearing system, the choice of stator shape depends on the need of which of its bearing characteristics are to be optimized. Moreover, the study suggests that it is advantageous to use parallel slider bearing owing to its maximum load-carrying capacity and least frictional force on its slider.

REFERENCES

1. Shliomis MI. 1972 Effective viscosity of magnetic suspensions. *Soviet Physics JETP*, 34(6):1291-1294.
2. Jenkins JT. 1971 Some simple flows of a para-magnetic fluid. *Journal de Physique*, 32: 931-938.
3. Jenkins JT. 1972 A theory of magnetic fluids. *Archiv for Rational Mechanics and Analysis*, 46(1): 42-60.
4. Huang W, Wang X. 2015 Ferrofluids lubrication : a status report. *Lubrication Science*, 28(1): 3-26.
5. Neuringer JL, Rosensweig RE. 1964 Ferrohydrodynamics. *The physics of fluids*, 7(12):1927-1937.
6. Tipei N. 1982 Theory of lubrication with ferrofluids: Application to short bearings. *Transactions of ASME*, 104:510-515.
7. Agrawal VK. 1986 Magnetic fluid based porous inclined slider bearing. *Wear*, 107:133-139.
8. Chi CQ, Wang ZS, Zhao PZ. 1990 Research on a new type of ferrofluid-lubricated journal bearing. *Journal of Magnetism and Magnetic Materials*, 85:257-260.
9. Prajapati BL. 1995 Magnetic-fluid-based porous squeeze films. *Journal of Magnetism and Magnetic Materials*, 149:97-100.
10. Shah RC, Bhat MV. 2004 Ferrofluid squeeze film in a long journal bearing. *Tribology International*, 37: 441-446.
11. Ahmad N, Singh JP. 2007 Magnetic fluid lubrication of porous-pivoted slider bearings with slip velocity. *Journal of Engineering Tribology*, 221: 609-613.
12. Shah RC, Patel NI. 2015 Impact of various and arbitrary porous structure in the study of squeeze step bearing lubricated with magnetic fluid considering variable magnetic field. *Journal of Engineering Tribology*, 229(5): 646-659.
13. Shah R C, Kataria RC. 2016 On the squeeze film characteristics between a sphere and a flat porous plate using ferrofluid. *Applied Mathematical Modelling*, 40: 2473-2484.
14. Shah RC, Patel DA. 2016 On the ferrofluid lubricated squeeze film characteristics between a rotating sphere and a radially rough plate. *Meccanica*, 51: 1973-1984.

15. Ram P, Verma PDS. 1999 Ferrofluid lubrication in porous inclined slider bearing. *Indian Journal of Pure & applied Mathematics*, 30(12): 1273-1281.
16. Maugin GA. 1980 The principle of virtual power : Application to coupled fields. *Acta Mechanica*, 35:1-70.
17. Shah RC, Bhat MV. 2002 Exponential Slider bearing lubricated with ferrofluid. *Mediterraneantrib Conference, Kayseri, Turkey*, 99-103.
18. Shah RC, Bhat MV. 2003 Lubrication of a slider bearing with magnetic fluid. *Journal of the Balkan Tribological Association*, 9(2): 280-284.
19. Shah RC, Patel DB. 2014 Magnetic fluid lubrication of porous pivoted slider bearing with slip and squeeze velocity. *International Journal of Industrial Mathematics*, 6(3): 199-206
20. Shukla JB, Kumar D. 1987 A theory for ferromagnetic lubrication. *Journal of Magnetism and Magnetic Materials*, 65: 375-378.
21. Shah RC, Bhat MV. 2005 Ferrofluid squeeze film between curved annular plates including rotation of magnetic particles. *Journal of Engineering Mathematics*, 51: 317- 324.
22. Shah RC, Parikh KS. 2014 Comparative study of ferrofluid lubricated various designed slider bearings considering rotation of magnetic particles and squeeze velocity. *International Journal of Theoretical and Mathematical Physics*, 4(2): 63-72.
23. Singh UP, Gupta RS. 2012 Dynamic performance characteristics of a curved slider bearing operating with ferrofluids. *Advances in Tribology*, Article ID 278723, 6 pages.
24. Lin JR. 2013 Dynamic characteristics of magnetic fluid based sliding bearings. *Mechanika*, 19(5): 554-558.
25. Khonsari MM, Booser ER. 2001 *Applied Tribology: Bearing design and lubrication*. John Wiley & Sons, Inc.
26. Szeri AZ. 1998 *Fluid film lubrication*. Cambridge University Press, Cambridge.

Bearing Designs	Inclined slider bearing	Exponential slider bearing	Secant slider bearing	Convex slider bearing	Parallel slider bearing
\bar{x}	0.569	0.568	0.664	0.569	0.500
\bar{W}	0.988	1.058	0.560	1.036	2.599

Table 3.1 Effect on \bar{x} with corresponding values of \bar{W} for different bearing designs for $\beta = 5.10$ and $\lambda = 0.171$

Bearing Designs	Inclined slider bearing	Exponential slider bearing	Secant slider bearing	Convex slider bearing	Parallel slider bearing
\bar{W}	0.988	1.058	0.560	1.036	2.598
% variation in \bar{W} as compared to 100% of \bar{h}_s	76.43(↑)	88.93(↑)	0	85.00(↑)	363.93(↑)

Table 3.2 Effect on \bar{W} for different bearing designs for $\beta = 5.10$ and $\lambda = 0.171$

Shliomis Model	For uniform transverse magnetic field [22]	For the present case when $\lambda = 171.0$	For the present case when $\lambda = 1710.0$
$\dot{h}_1 = 0$	0.0	0.0027	0.028

Table 3.3 Comparison of dimensionless load-carrying capacity \bar{W} for parallel slider bearing.

Bearing Designs	Inclined slider bearing	Exponential slider bearing	Secant slider bearing	Convex slider bearing	Parallel slider bearing
\bar{F}	1.200	1.235	1.106	1.227	1.019
% variation in \bar{F} as compared to 100% of \bar{h}_s	8.50(↑)	11.66(↑)	0	10.94(↑)	7.87(↓)

Table 3.4 Effect on \bar{F} for different bearing designs for $\beta = 5.10$ and $\lambda = 0.171$

Bearing Designs	Inclined slider bearing	Exponential slider bearing	Secant slider bearing	Convex slider bearing	Parallel slider bearing
\bar{f}	1.214	1.168	1.973	1.185	0.392
% variation in \bar{f} as compared to 100% of \bar{h}_s	38.47(↓)	40.80(↓)	0	39.94(↓)	80.13(↓)

Table 3.5 Effect on \bar{f} for different bearing designs for $\beta = 5.10$ and $\lambda = 0.171$

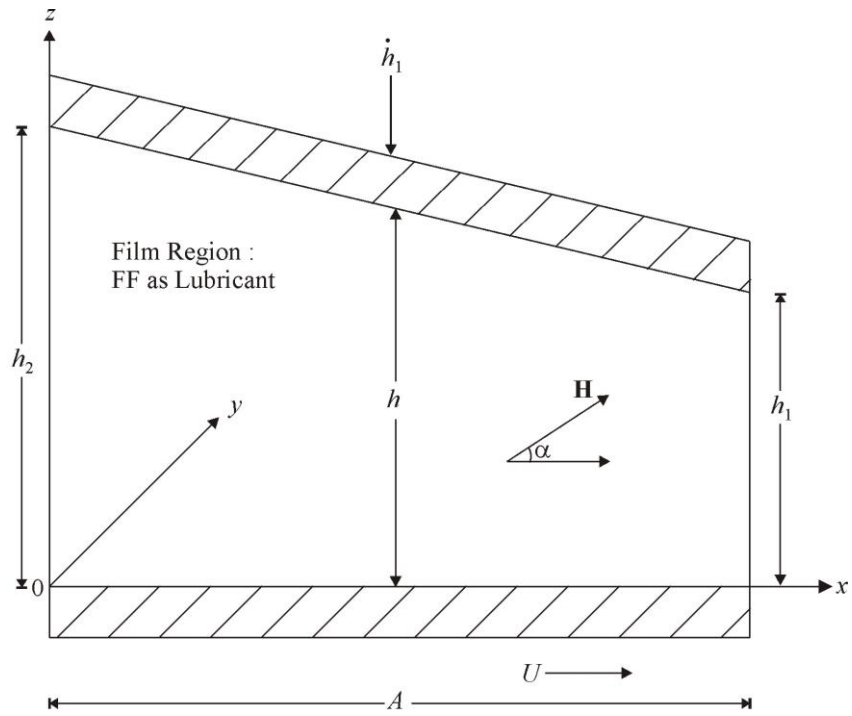


Figure 3.1 Inclined slider bearing

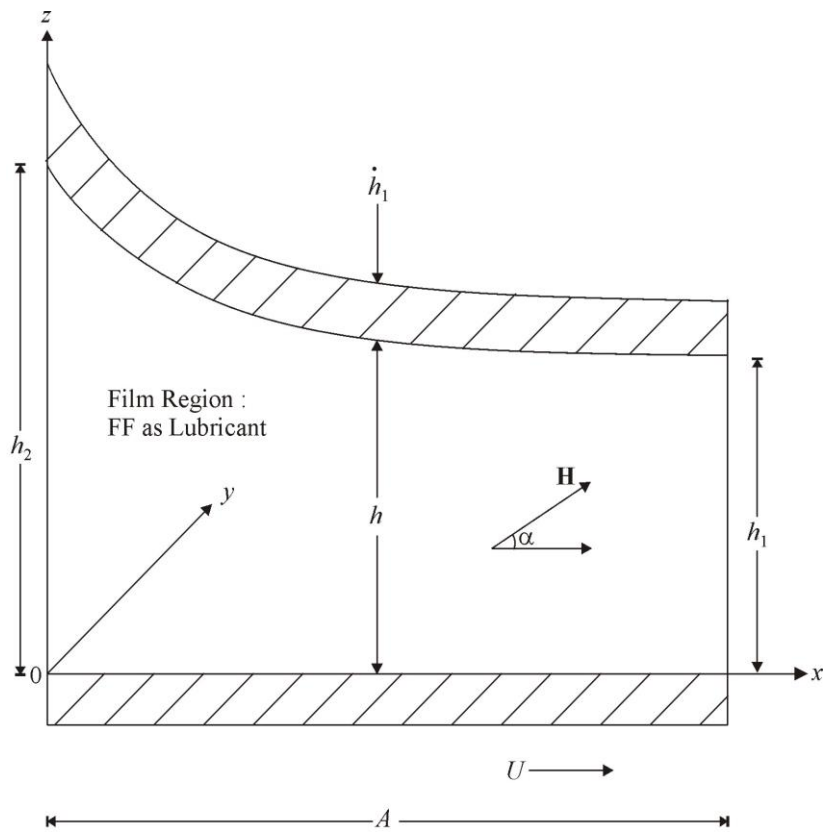


Figure 3.2 Exponential slider bearing

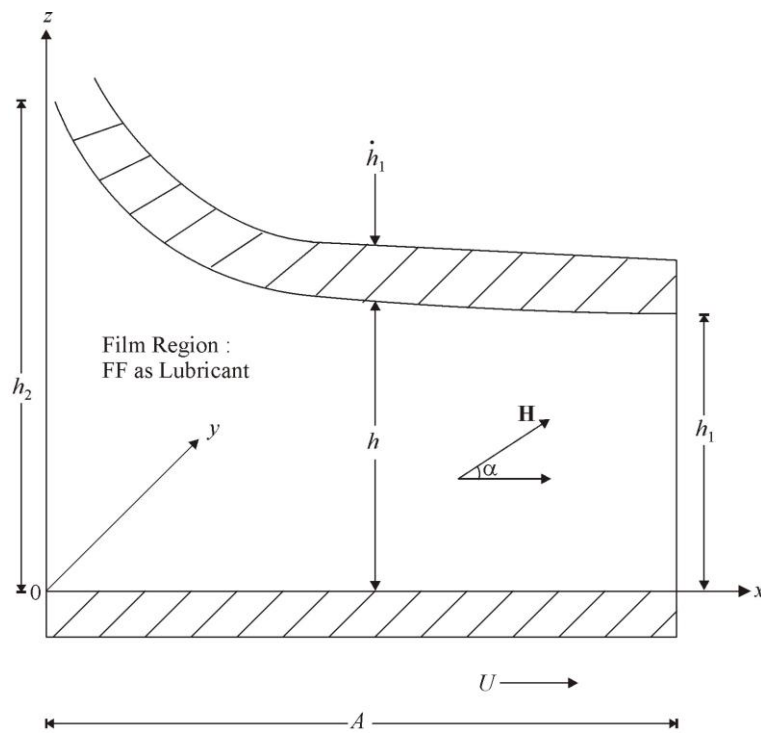


Figure 3.3 Secant slider bearing

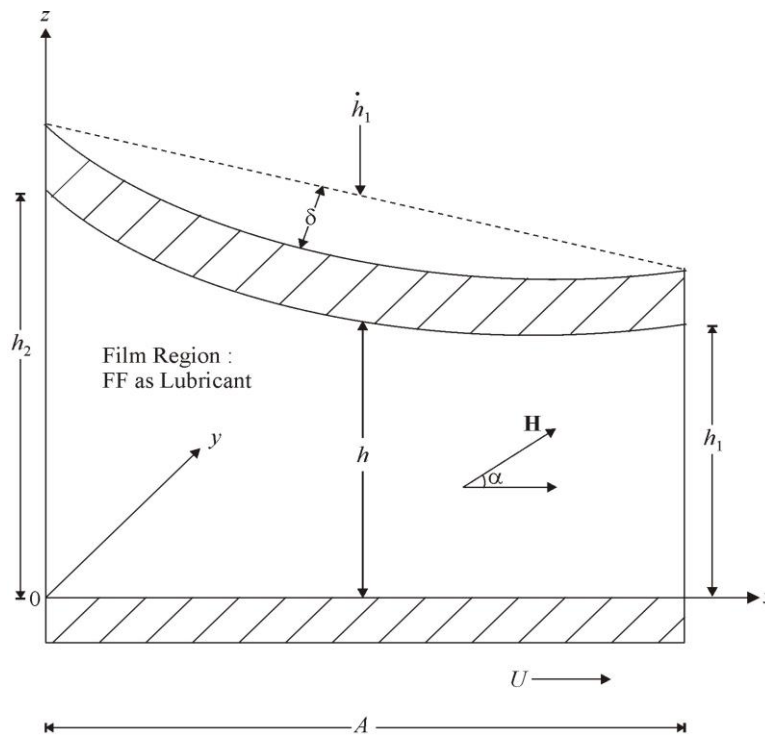


Figure 3.4 Convex slider bearing

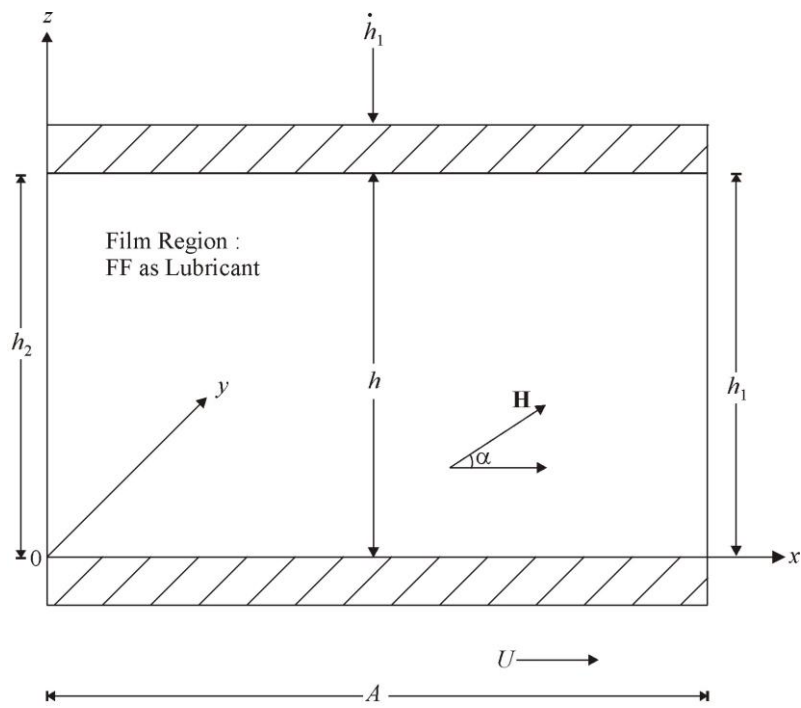


Figure 3.5 Parallel slider bearing

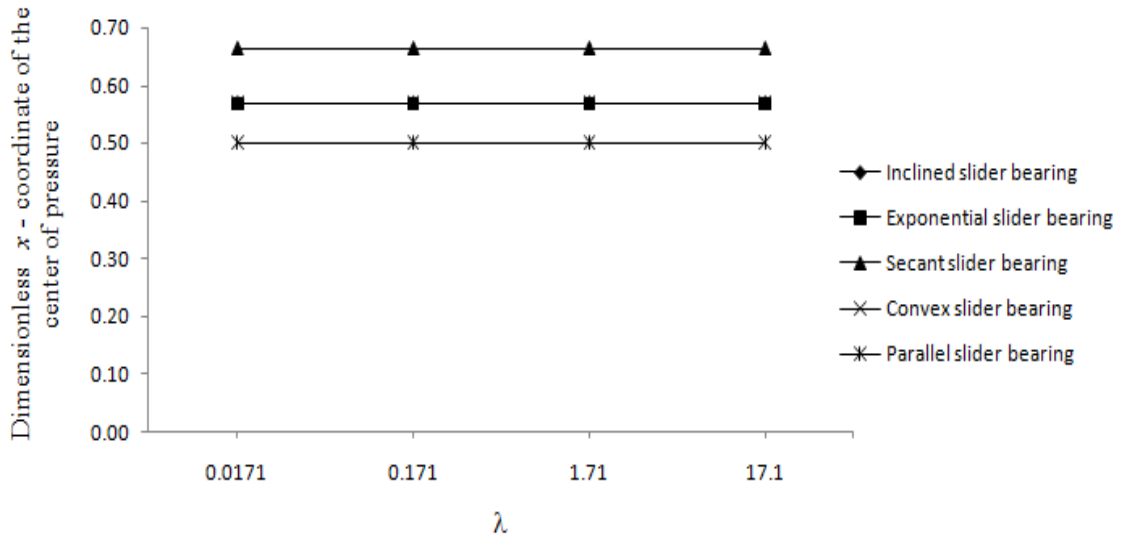


Figure 3.6 Dimensionless x – coordinate of the center of pressure (\bar{x}) for $\beta = 5.10$

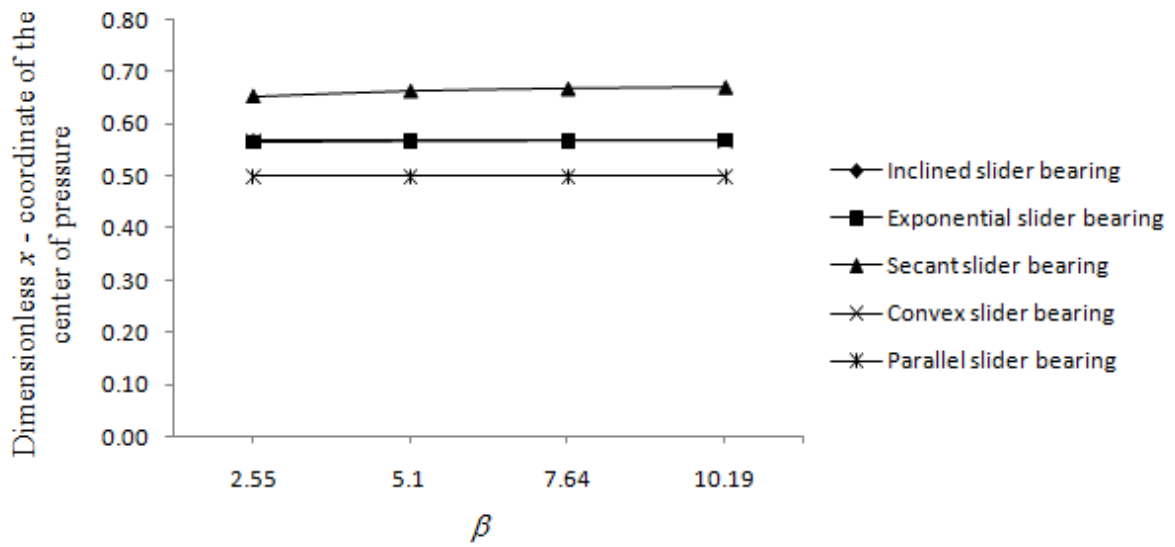


Figure 3.7 Dimensionless x – coordinate of the center of pressure (\bar{x}) for $\lambda = 0.171$

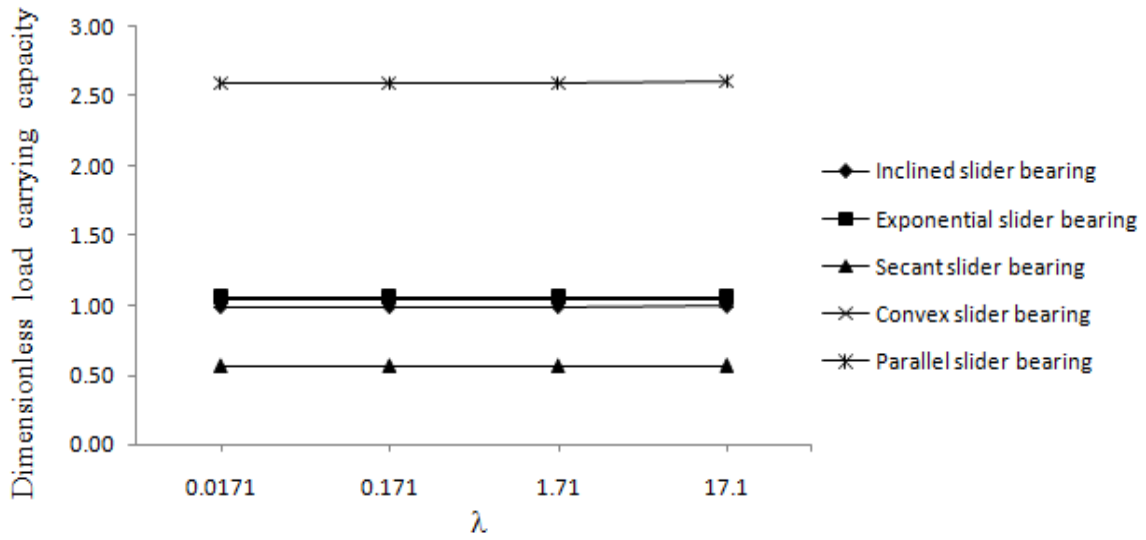


Figure 3.8 Dimensionless load-carrying capacity (\bar{W}) for $\beta = 5.10$

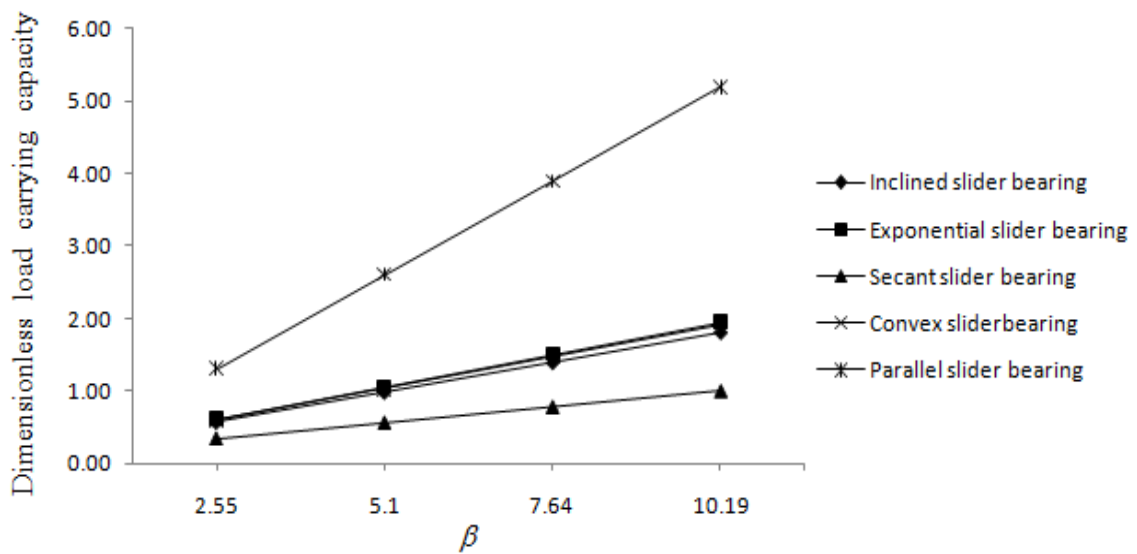


Figure 3.9 Dimensionless load-carrying capacity (\bar{W}) for $\lambda = 0.171$

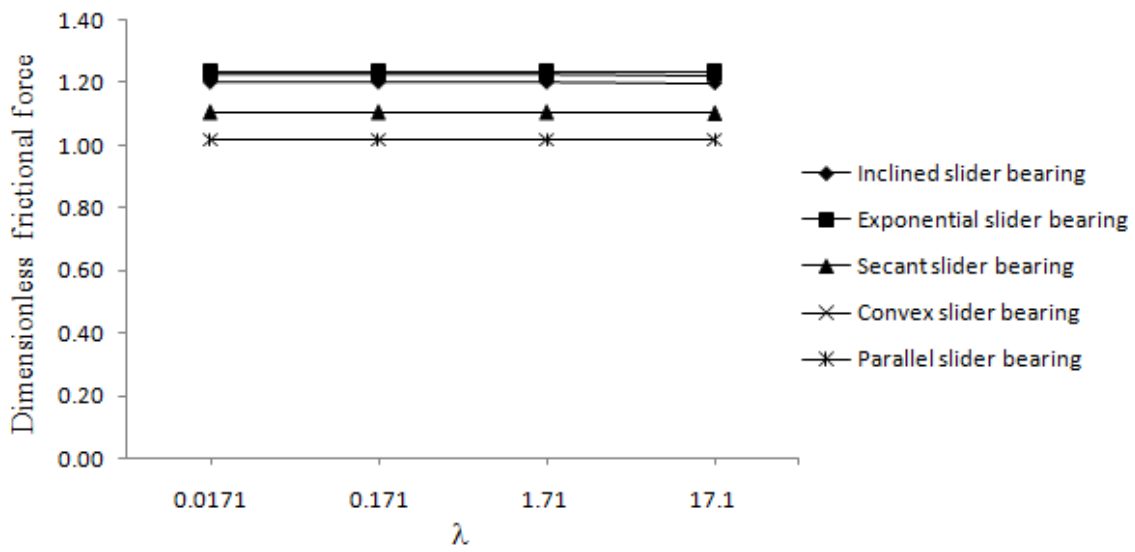


Figure 3.10 Dimensionless frictional force (\bar{F}) for $\beta = 5.10$.

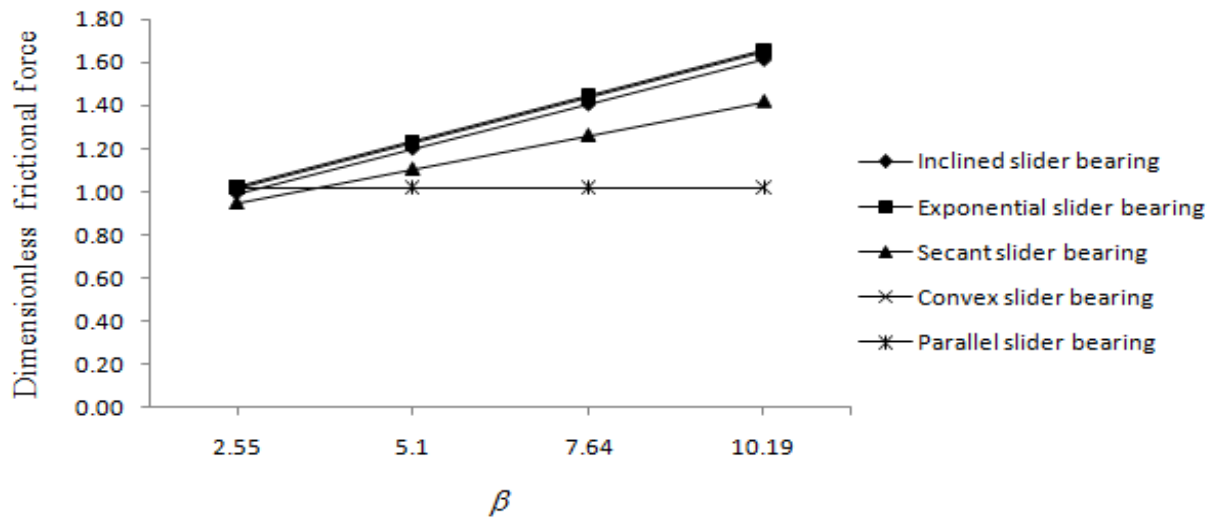


Figure 3.11 Dimensionless frictional force (\bar{F}) for $\lambda = 0.171$.

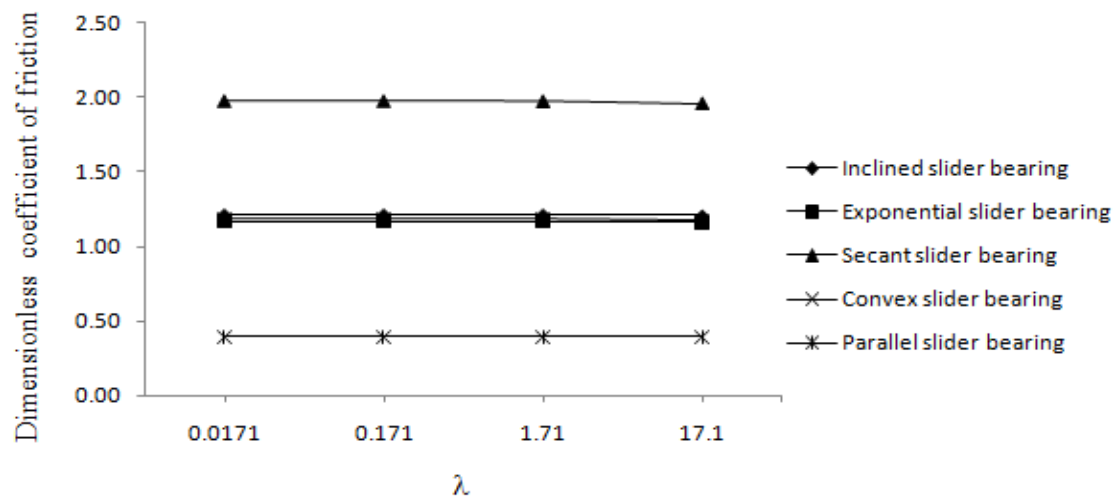


Figure 3.12 Dimensionless coefficient of friction (\bar{f}) for $\beta = 5.10$.

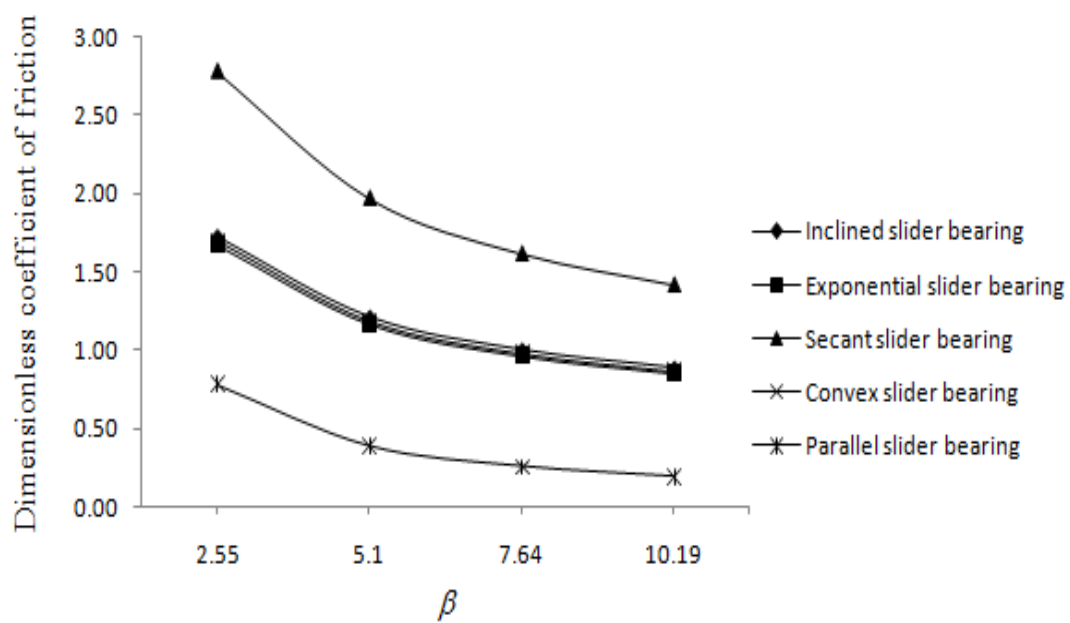


Figure 3.13 Dimensionless coefficient of friction (\bar{f}) for $\lambda = 0.171$.